

Bimetallic Cantilevers for a MEMS Thermal Actuator

Fischer J. Moseley, *Student Member, IEEE*

Abstract—A thermally actuated MEMS device is fabricated with a simple two-mask process. The device consists of a bimetallic cantilever with an onboard heater, where the deflection of the cantilever is caused by a change in device temperature. This deflection is measured by breaking down the air in the gap across the cantilever, and while little variation was shown in breakdown voltage, a physical means of explaining the results is provided.

Index Terms—MEMS Devices, Silicon Nitride, Thermal Sensors, Nanosensors

I. INTRODUCTION

MEMS devices have enjoyed a long history of success in sensing applications. But MEMS devices are also useful for micromanipulation, particularly in optical and biological applications. These devices allow for incredibly small displacements, but can be hard to design depending on the actuation mechanism. Electrostatically actuated devices are simple to fabricate, but can struggle to produce large forces. Magnetically actuated devices can require specialized embedding of micromagnets, and large chip areas and multiple layers to fabricate coils. Both electrostatic and magnetic devices are difficult to design for systems with multiple actuators, as the fields are usually not tightly confined. This causes interactions between actuators, which may require 3D field solvers to fully characterize. This is computationally expensive and unintuitive.

To overcome these fundamental limitations of electrostatic and magnetic actuation, this work seeks to investigate thermally actuated MEMS systems. Thermal systems are intuitive, easy to model, simple to fabricate, and produce higher forces than electrostatic or magnetic actuators. By fabricating a cantilevered bimetallic strip with an integrated heater, a single-degree-of-freedom thermal actuator is created, shown in Figure 1. As the device temperature changes, the metals forming the cantilever will expand at different rates, causing the beam to deflect.

II. METHODS

A. Device Design

The device was designed with two parts. The first is a bimetallic strip fixed to the wafer at one end, forming a cantilever. The cantilever is made with a layer of gold atop a layer of silicon nitride, under which a pit is dug to allow

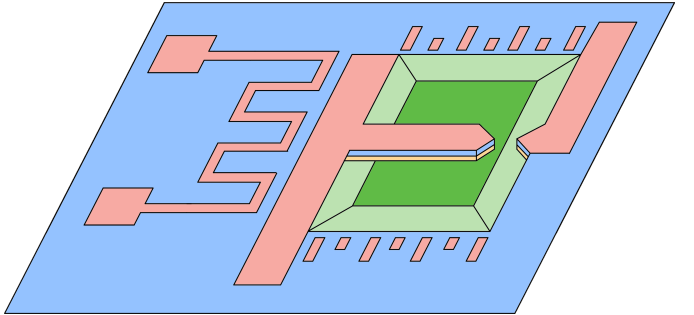


Fig. 1. False-color schematic of the device. The red, blue and orange layers represent the gold, nitride, and titanium layers. The silicon substrate is shown in green.

the cantilever to bend in either direction. Additionally, scale markers are placed at constant intervals along the side of the cantilever to provide a reference for optical measurement. For electrical measurement, contact pads are provided above and below the cantilever to connect to a probe station, allowing a voltage to be applied across the gap. The tip of the cantilever is pointed to increase the electric field at the gap, decreasing the breakdown voltage of the air within.

The second main feature of the device is an onboard heater adjacent to the cantilever. This was fabricated as a winding $15\mu\text{m}$ trace of gold, and functions as a resistor to heat the device. The device can be operated by controlling the current through the resistor, heating the device and causing the cantilever to deflect. Contact pads are also provided for the resistor, allowing it to be used on a probe station.

Because of the bulk micromachining techniques used, any number of devices can be fabricated on the same wafer for the same cost. This allowed for a range of actuators to be fabricated, varying a number of design parameters. The lengths of the cantilevers were varied from $50\text{-}500\mu\text{m}$, and the widths were varied from $50\text{-}100\mu\text{m}$. The gaps between the beam and the opposing electrode were varied from $1\text{-}5 \mu\text{m}$, and beams with both blunt and pointed tips were made.

B. Device Fabrication

The actuators were fabricated from a silicon wafer with a $1 \mu\text{m}$ layer of silicon nitride predeposited from an external contractor. After cleaning, electron beam evaporation was used to deposit a 10nm layer of titanium on the wafer. This serves as an adhesion layer for a 150nm layer of gold which sits atop it. After the metals were deposited, a $2 \mu\text{m}$ thick AZ3312 mask was patterned onto the gold surface, which was wet-etched in three stages. The etch consisted of a 15-second immersion in

Manuscript received May 9, 2022.

F. J. Moseley is with the Physics and Electrical Engineering departments at the Massachusetts Institute of Technology, Cambridge, MA 02139 USA (email: fischerm@mit.edu)

KI solution to etch the gold, followed by a rinse in deionized water. The wafer was then subjected to a 30-second immersion in HF to etch the underlying titanium layer. After another rinse, the surface resistance of the wafer was measured with an ohmmeter to ensure the gold and titanium had been removed, and only insulating nitride remained. This formed the metal structures on the device, including the heater coil and the top layer of the cantilever.

After burning off the remaining photoresist in an ashing, another $2\ \mu\text{m}$ AZ3312 mask was patterned on the wafer to form the geometry in the silicon nitride. The wafer was then dry-etched with RIE, exposing the silicon substrate underneath. The leftover photoresist was again stripped off in an ashing in preparation for the final etch. This took place in a 20% solution of KOH by weight, in which the wafers were left for an hour. KOH etches silicon anisotropically, causing it to undercut the cantilever and creating a pit below the device. After the etch, the cantilever is free of the wafer, and is free to deflect up and down in response to a changing temperature.

A few fabrication problems presented themselves, including:

- The titanium adhesion layer was partially etched by the KOH. This undercut the gold atop the titanium, causing small features to fully detach from the wafer as seen in Figure 2. The cantilevers themselves are relatively large ($50\text{-}100\ \mu\text{m}$) and didn't lift off the wafer, but the thin $15\ \mu\text{m}$ traces on the heater coils lifted off entirely. It is estimated that the undercut extended $10\text{-}12.5\ \mu\text{m}$ underneath the gold, as $20\ \mu\text{m}$ wide rectangles lifted off the wafer, while $25\ \mu\text{m}$ rectangles remained attached. The undercut wasn't visible via either SEM or optical microscope, as the 10nm titanium layer is too thin to resolve.
- The photoresist was underexposed during the lithography steps, leaving some unetched regions of gold on the surface. This is likely the result of a process change regarding photoresist thickness. During fabrication concerns existed surrounding the selectivity of AZ3312 in the KI and HF etches. As a result a thicker $2\ \mu\text{m}$ layer of AZ3312 was coated on the wafers rather than the standard $1\ \mu\text{m}$ layer. This was accommodated for when selecting the dosage on the direct-write laser used to expose the resist, but it is possible the dosage wasn't increased enough to compensate. As a result, the resist would be underexposed and some gold regions would remain on the device.
- The two masks were misaligned by around $4\ \mu\text{m}$, primarily in the forward-backward direction. This is most easily seen in the cantilever tips, as shown in Figure 3. This is unlikely to prevent the device from working entirely, but the shifted electrode locations change the device's behavior under electrical test.
- Undercutting of the gold and titanium during the KI and HF etches substantially increased the spacing of the airgap. In the case of the device shown in 3, the gap spacing was designed to be $5\ \mu\text{m}$ but is measured to be $8.6\ \mu\text{m}$ under the SEM - an undercut of $1.8\ \mu\text{m}$ on either side. This increased spacing substantially changes the device's behavior under electrical test.

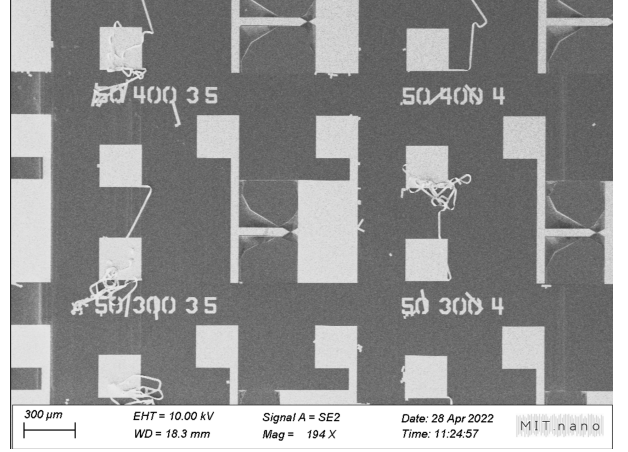


Fig. 2. The array of devices, as fabricated. The titanium undercutting has caused the device heaters and scale markers to lift off the device.

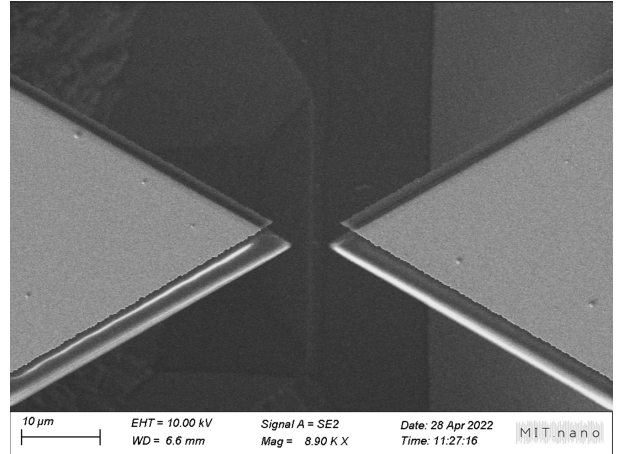


Fig. 3. The misalignment between the cantilever electrodes. The gap between the electrodes has been widened to $8.6\ \mu\text{m}$ from the originally patterned $5\ \mu\text{m}$ spacing.

C. Testing Setup

The performance of the device is measured by means of an electrical test and optical test. In the electrical experiment, the electrodes at either end of the device are sharply pointed and closely spaced such that a small voltage is sufficient to break down the air between them. The voltage required for this is a function of the spacing between electrodes, which is dependent on the device temperature. This provides an electrical means of determining electrode deflection, and also device temperature.

In the optical experiment, the device is heated by either running current through the onboard heater or with a hot plate. As the temperature increases, the tip deflects into the pit and goes out of focus relative to the body of the electrodes. The amount of deflection is measured, using the scale markers on the device as a reference to measure the displacement. This is repeated over a range of temperatures, either programmed with a hot plate or inferred from the heater current and temperature-dependent resistivity of gold.

Unfortunately, the optical test showed no deflection or change in gap size as the device temperature was raised to

200 °C. This is likely because the horizontal displacement of the beam is relatively small (around 1-2 μm) making it hard to resolve on the microscope. The rest of this work gives attention to the electrical test as a result.

D. Modelling

The deflection of the bimetallic strip is calculable from beam theory, and it bends with uniform curvature as it is heated or cooled. The curvature κ is determined by the temperature increase of the device along with the Young's modulus and thermal expansion coefficient of the constituent metals. This is provided by the following expressions:

$$\epsilon = (\alpha_1 - \alpha_2)\Delta T \quad (1)$$

$$\kappa = \frac{6E_1E_2(h_1 + h_2)h_1h_2\epsilon}{E_1^2h_1^4 + 4E_1E_2h_1^3h_2 + 6E_1E_2h_1^2h_2^2 + 4E_1E_2h_2^3h_1 + E_2^2h_2^4} \quad (2)$$

Where ϵ is the misfit strain between the metals, which is given by the thermal expansion coefficients of the metals α_1 and α_2 and the temperature difference ΔT . This strain is used to calculate the curvature κ , where E_1 and E_2 are the Young's moduli of the metals, and h_1 and h_2 are their respective thicknesses. [5] Values for material properties were taken from [4]. κ is the inverse of the radius of curvature, shown as R in Figure 4.

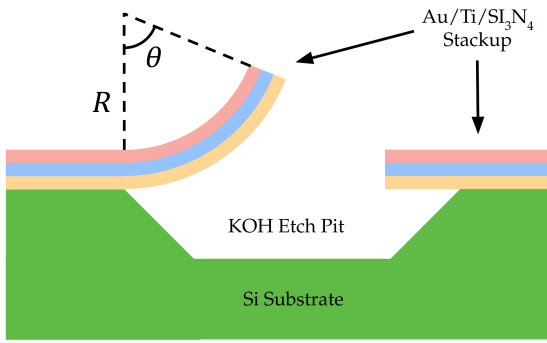


Fig. 4. Cross-section of the device. The red/green/orange layers represent the gold/titanium/silicon nitride layers, and the bulk silicon substrate is shown in blue.

Given the radius of curvature, it is possible to calculate the gap spacing from geometry. If the unbent length of the beam is taken to be l , then the angle of the resulting arc θ can be used to calculate the vertical and horizontal deflection of the beam:

$$\theta = l/R \quad (3)$$

$$\Delta x = l - R \sin \theta \quad (4)$$

$$\Delta y = R - R \cos \theta \quad (5)$$

From this, the distance between electrodes is calculated.

With the airgap spacing modelled as a function of temperature, attention was turned to predicting the breakdown

voltage of the airgap from its spacing. This requires invoking a modified form Paschen's Law, as the standard breakdown strength of air (3MV/m) only holds at distances in excess of around 100 μm, well beyond the airgap spacing of the devices presented here. Paschen's Law predicts breakdown voltages in air at atmospheric pressure for gaps in the 7-100 μm range, but produces unphysical results as the gap spacing is taken to zero, predicting infinite breakdown voltage. Reference [8] aggregates a collection of published breakdown voltages at micrometer spacings, and provides a piecewise empirical fit to a series of published data. This fit is shown in Figure 5, and is used to compute the breakdown voltage required as a function of temperature, which is then represented in Figure 6.

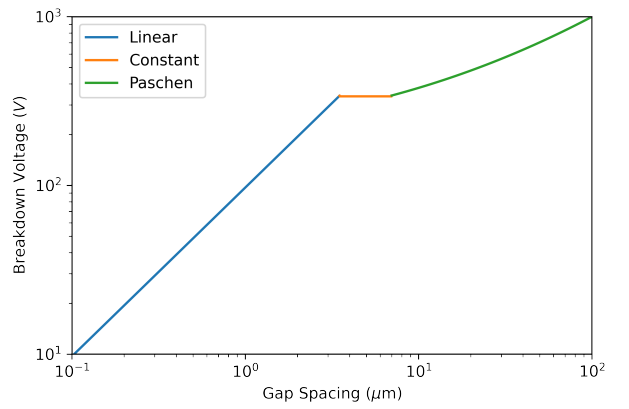


Fig. 5. The breakdown voltage required to bridge the gap, as a function of the gap size. The linear region, represented in blue, shows a linear relationship between breakdown voltage and gap size for distances less than 3.5 μm. The constant region, represented in orange, shows no variation in discharge voltage - it takes 337V to breakdown across both a 3.5 μm and a 7 μm gap. The discharge voltage eventually follows Paschen's Law in the green region of the plot, representing gaps larger than 7 μm. The green curve asymptotically approaches the accepted 3MV/m value as the distance increases to the right.

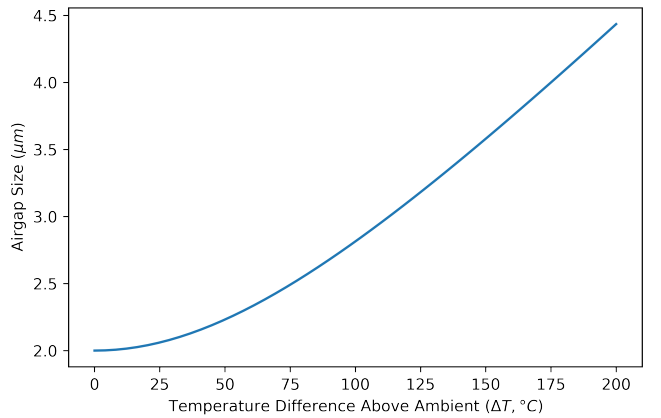


Fig. 6. Deflection of the beam under temperature, with predicted results using the beam deflection formula given in Equations 1 and 2 and the gap spacing

This breakdown voltage is taken as an overestimate, as the Coulomb attraction between the two electrodes will decrease

the separation between them. This attractive force proved difficult to model despite the author's best efforts in Ansys Maxwell. Given the geometry of the device, an analytical model of the attraction is very difficult to obtain, so one is not provided here.

III. RESULTS

It was found that the electrical breakdown testing was destructive, as seen in Figure 7. Although most of the device was completely obliterated during testing, this was little obstacle due to the number of devices onboard. This allowed for 21 devices to be tested, with breakdown voltages plotted in Figure 8.

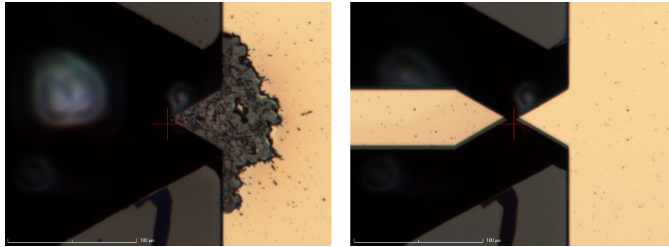


Fig. 7. Close-up picture of the device before and after a discharge test. The gold layer on the right electrode is partially removed, while the cantilever beam has been completely obliterated. Although not shown here, damage was sustained on other parts of the device, including the contact pads and electrode bodies.

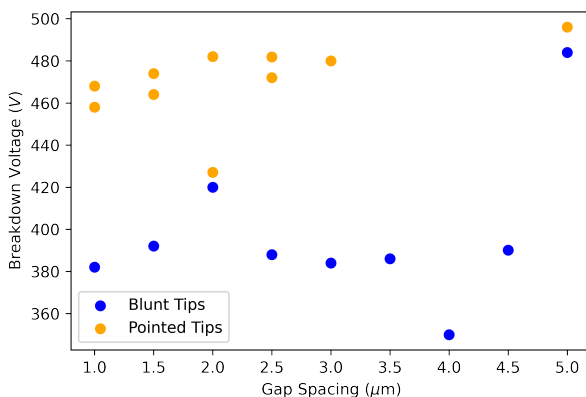


Fig. 8. The measured breakdown voltages as a function of gap size (as designed, not necessarily fabricated). Both a blunt tip and a pointed tip were tested.

Interestingly, the breakdown voltage doesn't vary much over the gap size. This is likely because the devices were accidentally designed to partially operate in the constant region of the breakdown-gap curve. The gap range shown in Figure 6 is $2\text{--}4\mu\text{m}$, which partially overlaps the constant region of the breakdown curve (Figure 5). Although designed to partially operate in this region, the fabricated devices displayed an increased spacing between electrodes (Figure 3), likely sending the entire device operating region of the device into the constant region of the breakdown curve. As a result, any deflection would be immeasurable, as the gaps would produce the same breakdown voltage regardless of their spacing.

IV. CONCLUSION

While the principles behind the actuator are sound, the electrical testing performed on the devices was both destructive and ineffective. Although the mechanism behind the test's ineffectiveness is known, it prevented measurement of actuator performance and further work will require a new testing method. Some modifications will also need to be made to the process to avoid the Ti/KOH incompatibility, and it could be productive to test devices without the titanium adhesion layer.

ACKNOWLEDGMENT

F. J. Moseley thanks the 6.152 course staff for their endless help in the fab. In particular, Jorg spent a considerable amount time on Zoom consulting about the project, and the results here wouldn't have been possible without him. Thanks also to Scott and Kurt for their guidance in the fab and for putting up with endless questions on early Friday mornings.

REFERENCES

- [1] H. Seidel, "Anisotropic Etching of Crystalline Silicon in Alkaline Solutions" *Journal of The Electrochemical Society* vol. 137, no. 11 pp. 3612–3626. November 1990. DOI 137(17):3612-3626.
- [2] J. del Alamo et al., "Lab 2 Notes: 6.152 Spring 2022," *Massachusetts Institute of Technology* Cambridge, MA, USA, 2022.
- [3] S. D. Senturia, "Dissipation and the Thermal Energy Domain" in *Microsystem Design*, 1st ed. Boston, MA, USA: Kluwer Academic Publishers, 2001, ch. 11 267–296.
- [4] W.M. Haynes et al., "Electrical Resistivity of Pure Metals" in *CRC Handbook of Chemistry and Physics* 95th ed. New York, NY, USA: CRC Press, 2014, pp. 12-41
- [5] MathWorks, "Thermal Deflection of a Bimetallic Beam" *MATLAB Documentation* Natick, MA, USA. Retrieved 21 April 2022.
- [6] H. Conrad et al., "A small-gap electrostatic micro-actuator for large deflections" in *Nature Communications* December 2015. DOI 10.1038/ncomms10078
- [7] D. Niarchos, "Magnetic MEMS: key issues and some applications" in *Sensors and Actuators A* vol. 109, pp. 166–173. December 2003. DOI 10.1016/j.sna.2003.09.010
- [8] V. Babrauskas, "Arc Breakdown in Air over Very Small Gap Distances" in *Interflam* vol. 2, pp. 1489–1498. January 2013.